ENCIT 2002

IX CONGRESSO BRASILEIRO DE ENGENHARIA E CIÊNCIAS TÉRMICAS

9th BRAZILIAN CONGRESS OF THERMAL ENGINEERING AND SCIENCES

ABCM

Paper CIT02-0804

ASSESSMENT OF DIFFERENT NUMERICAL SCHEMES AND GRID REFINEMENT FOR HYDRODYNAMIC STABILITY SIMULATIONS

Leandro F. de Souza
Instituto Tecnológico de Aeronáutica
Pç Mal. Eduardo Gomes, 50 - São José dos Campos, SP - 12228 900, Brazil
lefraso@zipmail.com.br

Márcio T. Mendonça
Centro Técnico Aeroespacial, Instituto de Aeronáutica e Espaço
Pç Mal. Eduardo Gomes, 50 - São José dos Campos, SP - 12228 904, Brazil
marcio_tm@yahoo.com

Marcello A. Faraco de Medeiros
USP - Universidade de São Paulo, São Carlos
Escola de Engenharia de São Carlos - Departamento de Engenharia Aeronáutica
Av. Trabalhador São Carlense, 400 - São Carlos, SP - 13566-590, Brazil
marcello@sc.usp.br

Abstract. *This paper presents various finite differences schemes and compare their ability to simulate instability waves in a given flow field. The governing equations for two-dimensional, incompressible flows are derived in vorticity-velocity formulation. Four different space discretization schemes are tested, namely, a 2^{nd} order central differences, a 4^{th} order central differences, a 4^{th} order compact scheme and a 6^{th} order compact scheme. In time a classic 4^{th} order Runge-Kutta scheme is used. The influence of grid refinement in the streamwise and normal directions are evaluated. The results are compared against linear stability theory for the evolution of small amplitude Tollmien-Schlichting waves in a plane Poiseuille flow. Both the amplification rate and the wavenumber are considered as verification parameters, showing the degree of dissipation and dispersion introduced by the different numerical schemes. The results confirm that high order schemes are necessary for studying the hydrodynamic instabilities of this flow.*

Key words: *High resolution finite differences, Compact differences schemes, Vorticity-velocity formulation, Hydrodynamic instability, Laminar flow transition to turbulence.*

1. Introduction

In many applications the ability to predict whether a given flow is laminar or turbulent is crucial, since heat transfer rates and skin friction coefficients are much larger in turbulent flows. The knowledge of the flow regime, laminar, transitional or turbulent, helps the correct design of aerodynamic surfaces or cooling systems. In certain situations it is even desirable to control the evolution of a laminar flow in order to delay transition and reduce viscous drag (Joslin, 1998b, Joslin, 1998a, Davies et al., 1999).

The Direct Numerical Simulation (DNS) of the Navier-Stokes equations to study stability and transition is becoming more feasible with the increasing capacity of modern computational resources. Different approaches have been presented in the literature (Laurien and Kleiser, 1989, Biringen and Laurien, 1991, Spalart, 1989, Gmelin et al., 1999, Meyer et al., 1999, Zhong, 1999, Whang and Zhong, 1999, Hu and Zhong, 1999, Guschin et al., 1999) and a common factor among them is the need for high resolution discretization methods (Zang et al., 1989). This is because the numerical study of hydrodynamic stability and transition to turbulence requires the correct representation of a range of spatial and time scales. Spectral methods can be used to assure that all relevant scales are captured, but higher order finite difference are also able to represent short length scales with good accuracy. Lele (Lele, 1992) emphasizes the importance of using high order methods for these flows and shows schemes for first and second derivatives of 2^{nd} to 10^{th} order. Mahesh (Mahesh, 1998) shows higher order finite difference schemes, introducing a method that is more accurate than the standard Padé schemes using the same stencil. The disadvantage of this method is that it requires the solution of first and second derivatives simultaneously. Hirsh (Hirsh, 1975) and Adam (Adam, 1977) also discusses some advantages of a fourth order compact methods compared to standard methods.

Another relevant aspect to be considered in direct numerical simulation of stability and transition problems is grid refinement. Coarse-grid simulations can introduce both artificial dissipation and spurious oscillations in the flow.

In the current study, a formulation based on the vorticity-velocity variables (Messing et al., 1999, Fezer and Kloker, 1999, Stemmer and Kloker, 1999, Wassermann and Kloker, 1999, Wassermann and Kloker, 1998, Zhang and Fasel, 1999) was adopted. The growth of instability modes in a two-dimensional Poiseuille incompressible flow is simulated. The disturbances introduced in the flow field can grow, decay or stay constant depending on the Reynolds number and frequency.

The emphasis in this paper is on inferring what degree of resolution is needed to capture reliably the instantaneous structure of a disturbed flow. In Section 2 the governing equations are derived, and the details of the numerical methods are described. The time and spatial discretization used is also shown in this section. Four different schemes used to discretize spatial derivatives are presented, namely, 2^{nd} order explicit central derivatives, 4^{th} order explicit central derivatives, 4^{th} order implicit (compact) central derivatives and 6^{th} order implicit (compact) central derivatives. Section 3 presents details of the linear stability analysis for plane Poiseuille flows. In Section 4 the propagation of a stable, a neutral and a unstable disturbances using a 6^{th} order compact method is given. Then, simulations using the other 3 approaches for spatial derivatives were also given for a neutral disturbance. Section 5 presents the conclusions and final comments.

2. Formulation and numerical method

For the numerical solution, the Navier-Stokes equations were written in vorticity-velocity formulation. The vorticity in the spanwise direction, denoted by w_z, is:

$$w_z = \frac{\partial u}{\partial y} - \frac{\partial v}{\partial x}. \tag{1}$$

The vorticity transport equation is:

$$\frac{\partial w_z}{\partial t} + \frac{\partial u w_z}{\partial x} + \frac{\partial v w_z}{\partial y} = \frac{1}{Re}\left(\frac{\partial^2 w_z}{\partial x^2} + \frac{\partial^2 w_z}{\partial y^2}\right). \tag{2}$$

The continuity equation is:

$$\frac{\partial u}{\partial x} + \frac{\partial v}{\partial y} = 0. \tag{3}$$

From the vorticity equation(1) and the continuity equation (3) a Poisson-type equation for the v velocity can be derived:

$$\frac{\partial^2 v}{\partial x^2} + \frac{\partial^2 v}{\partial y^2} = -\frac{\partial w_z}{\partial x}. \tag{4}$$

Equations (2), (3) and (4) were solved numerically by the schemes described below.
The solution was marched in time according to the following steps:

1. Impose initial conditions for u, v and w_z compatible with each other;
2. Introduce disturbance at inlet boundary, using eigenfunctions obtained from solving the Orr-Sommerfeld Equation for the Poiseuille flow;
3. Calculate the vorticity from the vorticity transport equation (2), for time $t + dt$;
4. Calculate v velocity from the Poisson equation (4);
5. Calculate u velocity from the continuity equation (3);
6. Calculate the vorticity generation at the wall for the new velocity distribution;
7. return to the second step until the desired integration time is reached.

The time derivative in the vorticity transport equation is discretized with a classical 4^{th} order Runge-Kutta integration scheme (Ferziger and Peric, 1997). For each intermediate step in the Runge-Kutta integration it is necessary to update the velocity field and the vorticity at the wall by taking steps 4 to 6 in the scheme described above.

For the spatial derivatives four different schemes were used. Bellow the discretization used for each method is presented, taking the derivative in x direction as an example, since it is analogous for the y derivatives. The letter i represents the grid position in x direction, which varies from 1 to N.

2^{nd} order derivatives: For $1 < i < N$:

$$\frac{\partial f}{\partial x}_i = \frac{f_{i+1} - f_{i-1}}{2dx} + O(dx^2) \tag{5}$$

$$\frac{\partial^2 f}{\partial x^2}_i = \frac{f_{i+1} - 2f_i + f_{i-1}}{dx^2} + O(dx^2) \tag{6}$$

For $i = 1$:

$$\frac{\partial f}{\partial x}_1 = \frac{-3f_1 + 4f_2 - f_3}{2dx} + O(dx^2) \tag{7}$$

$$\frac{\partial^2 f}{\partial x^2}_1 = \frac{6f_1 - 15f_2 + 12f_3 - 3f_4}{dx^2} + O(dx^2) \tag{8}$$

For $i = N$:

$$\frac{\partial f}{\partial x}_N = \frac{3f_N - 4f_{N-1} + f_{N-2}}{2dx} + O(dx^2) \tag{9}$$

$$\frac{\partial^2 f}{\partial x^2}_N = \frac{6f_N - 15f_{N-1} + 12f_{N-2} - 3f_{N-3}}{dx^2} + O(dx^2) \tag{10}$$

4th order explicit derivatives: For $2 < i < N - 1$:

$$\frac{\partial f}{\partial x}_i = \frac{f_{i-2} - 8f_{i-1} + 8f_{i+1} - f_{i+2}}{12dx} + O(dx^4) \tag{11}$$

$$\frac{\partial^2 f}{\partial x^2}_i = \frac{-f_{i-2} + 16f_{i-1} - 30f_i + 16f_{i+1} - f_{i+2}}{12dx^2} + O(dx^4) \tag{12}$$

For $i = 1$:

$$\frac{\partial f}{\partial x}_1 = \frac{-50f_1 + 96f_2 - 72f_3 + 32f_4 - 6f5}{24dx} + O(dx^4) \tag{13}$$

$$\frac{\partial^2 f}{\partial x^2}_1 = \frac{225f_1 - 770f_2 + 1070f_3 - 780f_4 + 305f_5 - 50f_6}{60dx^2} + O(dx^4) \tag{14}$$

For $i = 2$:

$$\frac{\partial f}{\partial x}_2 = \frac{-6f_1 - 20f_2 + 36f_3 - 12f_4 + 2f5}{24dx} + O(dx^4) \tag{15}$$

$$\frac{\partial^2 f}{\partial x^2}_2 = \frac{50f_1 - 75f_2 - 20f_3 + 70f_4 - 30f_5 + 5f_6}{60dx^2} + O(dx^4) \tag{16}$$

$$\frac{\partial^2 f}{\partial x^2}_2 = \frac{11f_1 - 20f_2 + 6f_3 + 4f_4 - f_5}{12dx^2} + O(dx^3) \tag{17}$$

The use of a 4^{th} and 3^{rd} order approximations for $i = 2$ and $i = N - 1$ is discussed in the section considering the numerical results. The approximations for $i = N$, and $i = N - 1$ are analogous to the approximations for $i = 1$ and $i = 2$, the only change is the sign of the first derivative, as one can observe in the approximations of second order accuracy.

4th order implicit derivatives: To find the values of implicit derivatives a matrix must be solved, where all the derivatives in a grid line are solved simultaneously. The matrix for the first derivatives is:

$$\begin{bmatrix} 1 & 3 & & & & & & & \\ 1 & 4 & 1 & & & & & & \\ & \cdot & \cdot & \cdot & & & & & \\ & & & 1 & 4 & 1 & & & \\ & & & & \cdot & \cdot & \cdot & & \\ & & & & & & 1 & 4 & 1 \\ & & & & & & & 3 & 1 \end{bmatrix} \begin{bmatrix} f'_1 \\ f'_2 \\ \cdot \\ f'_i \\ \cdot \\ f'_{N-1} \\ f'_N \end{bmatrix} = \begin{bmatrix} \frac{1}{dx}(-17f_1 + 9f_2 + 9f_3 - f_4) \\ \frac{3}{6dx}(-f_1 + f_3) \\ \cdot \\ \frac{3}{dx}(-f_{i-1} + f_{i+1}) \\ \cdot \\ \frac{3}{dx}(-f_{N-2} + f_N) \\ \frac{1}{6dx}17f_N - 9f_{N-1} - 9f_{N-2} + f_{N-3}) \end{bmatrix}. \quad (18)$$

The matrix for the second derivatives is:

$$\begin{bmatrix} 1 & 11 & & & & & & & \\ 1 & 10 & 1 & & & & & & \\ & \cdot & \cdot & \cdot & & & & & \\ & & & 1 & 10 & 1 & & & \\ & & & & \cdot & \cdot & \cdot & & \\ & & & & & & 1 & 10 & 1 \\ & & & & & & & 11 & 1 \end{bmatrix} \begin{bmatrix} f''_1 \\ f''_2 \\ \cdot \\ f''_i \\ \cdot \\ f''_{N-1} \\ f''_N \end{bmatrix} = \begin{bmatrix} \frac{1}{3dx^2}(39f_1 - 8f_2 + 45f_3 - 3f_4) \\ \frac{12}{dx^2}(f_1 - 2f_2 + f_3) \\ \cdot \\ \frac{12}{dx^2}(f_{i-1} - 2f_i + f_{i+1}) \\ \cdot \\ \frac{12}{dx^2}(f_{N-2} - 2f_{N-1} + f_N) \\ \frac{1}{3dx^2}(39f_N - 81f_{N-1} + 45f_{N-2} - 3f_{N-3}) \end{bmatrix}. \quad (19)$$

6^{th} **order implicit (compact) derivatives:** The differences between the scheme used in this work and the 6^{th} order approximations shown by Lele (Lele, 1992) is in the discretization of the boundary and near boundary points. At the boundaries, a 3^{rd} order approximation is proposed by Lele, whereas for points near the boundaries he proposed a 4^{th} order approximation. In the current work a 5^{th} order approximation for the boundary points is adopted. For points near the boundaries, a 6^{th} order approximation was used.

The details of the discretization scheme were as follows.

For points at the boundary, $i = 1$:

$$f'_1 + 4f'_2 = \frac{1}{24dx}(-74f_1 + 16f_2 + 72f_3 - 16f_4 + 2f_5) + O(dx^5). \quad (20)$$

For the first point next to the boundary, $i = 2$:

$$f'_1 + 6f'_2 + 2f'_3 = \frac{1}{120dx}(-406f_1 - 300f_2 + 760f_3 - 80f_4 + 30f_5 - 4f_6) + O(dx^6). \quad (21)$$

For the points near other boundaries, $i = N$ and $i = N - 1$, similar approximations were used.

For the interior points, a 6^{th} order Padé approximation was used:

$$f'_{i-1} + 3f'_i + f'_{i+1} = \frac{1}{12dx}(-f_{i-2} - 28f_{i-1} + 28f_{i+1} + f_{i+2}) + O(dx^6). \quad (22)$$

The resulting linear algebraic system of equations in matrix form reads:

$$\begin{bmatrix} 1 & 4 & & & & & & \\ 1 & 6 & 2 & & & & & \\ & \cdot & \cdot & \cdot & & & & \\ & & & 1 & 3 & 1 & & \\ & & & & \cdot & \cdot & \cdot & \\ & & & & & 2 & 6 & 1 \\ & & & & & & 4 & 1 \end{bmatrix} \begin{bmatrix} f'_1 \\ f'_2 \\ \cdot \\ f'_i \\ \cdot \\ f'_{N-1} \\ f'_N \end{bmatrix} = \begin{bmatrix} \frac{1}{24dx}(-74f_1 + 16f_2 + 72f_3 - 16f_4 + 2f_5) \\ \frac{1}{120dx}(-406f_1 - 300f_2 + 760f_3 - 80f_4 + 30f_5 - 4f_6) \\ \cdot \\ \frac{1}{120dx}(-f_{i-2} - 28f_{i-1} + 28f_{i+1} + f_{i+2}) \\ \cdot \\ \frac{(406f_N + 300f_{N-1} - 760f_{N-2} + 80f_{N-3} - 30f_{N-4} + 4f_{N-5})}{120dx} \\ \frac{1}{120dx}(74f_N - 16f_{N-1} - 72f_{N-2} + 16f_{N-3} - 2f_{N-4}) \end{bmatrix}. \quad (23)$$

The second derivative, at the boundary, $i = 1$, were discretized using a 5^{th} order asymmetric approximation:

$$13f''_1 + 137f''_2 = \frac{1}{120dx^2}(9775f_1 - 20285f_2 + 11170f_3 - 550f_4 - 145f_5 + 36f_6) + O(dx^5). \quad (24)$$

The first point near the boundary, $i = 2$, used a 6^{th} order asymmetric approximation:

$$\begin{aligned} f_1'' \quad + \quad & 12f_2'' + 3f_3'' = \\ & \frac{1}{360dx^2}(4834f_1 - 8424f_2 + 1890f_3 + 2320f_4 - 810f_5 + 216f_6 - 26f_7) + O(dx^6) \end{aligned} \tag{25}$$

The interior points used a 6^{th} order Padé approximation:

$$2f_{i-1}'' + 11f_i'' + 2f_{i+1}'' = \frac{1}{4dx^2}(3f_{i-2} + 48f_{i-1} - 102f_i + 48f_{i+1} + 3f_{i+2}) + O(dx^6). \tag{26}$$

For the points near other boundaries, $i = N$ and $i = N - 1$, similar approximations to the ones used for points $i = 1$ e $i = 2$ are used. The resulting linear algebraic system of equations in matrix form reads:

$$\begin{bmatrix} 13 & 137 & & & & & & & \\ 1 & 12 & 3 & & & & & & \\ & \cdot & \cdot & \cdot & & & & & \\ & & & 2 & 11 & 2 & & & \\ & & & & & \cdot & \cdot & \cdot & \\ & & & & & & 3 & 12 & 1 \\ & & & & & & & 137 & 13 \end{bmatrix} \begin{bmatrix} f_1'' \\ f_2'' \\ \cdot \\ f_i'' \\ \cdot \\ f_{N-1}'' \\ f_N'' \end{bmatrix} =$$

$$\begin{bmatrix} \frac{1}{120dx^2}(9775f_1 - 20285f_2 + 11170f_3 - 550f_4 - 145f_5 + 36f_6) \\ \frac{1}{360dx^2}(4834f_1 - 8424f_2 + 1890f_3 + 2320f_4 - 810f_5 + 216f_6 - 26f_7) \\ \cdot \\ \frac{1}{4dx^2}(3f_{i-2} + 48f_{i-1} - 102f_i + 48f_{i+1} + 3f_{i+2}) \\ \cdot \\ \frac{1}{360dx^2}(4834f_N - 8424f_{N-1} + 1890f_{N-2} + 2320f_{N-3} - 810f_{N-4} + 216f_{N-5} - 26f_{N-6}) \\ \frac{1}{120dx^2}(9775f_N - 20285f_{N-1} + 11170f_{N-2} - 550f_{N-3} - 145f_{N-4} + 36f_{N-5}) \end{bmatrix}. \tag{27}$$

To solve the Poisson equation, a Line Successive Over-Relaxation method (LSOR) was used. The method is a combination of a 4^{th} order explicit approximations in x direction and 6^{th} order compact approximations in y direction. Some tests were made using a full 6^{th} order compact approximations method and no relevant differences in the results were found. The full 6^{th} order compact method required a larger computational effort, therefore, in this simulations, the combination method was adopted.

Three types of boundary conditions needed to be specified: inflow boundary condition, wall boundary condition and outflow boundary condition.

At the inlet, the boundary condition was specified by superposing a small disturbance on top of the laminar Poiseuille flow velocity $U(y)$ and vorticity $W_z(y)$ distributions.

$$\begin{aligned} u(x_0, y, t) &= U(y) + u'(x_0, y, t), \\ v(x_0, y, t) &= v'(x_0, y, t), \\ w_z(x_0, y, t) &= W_z(y) + w_z'(x_0, y, t). \end{aligned} \tag{28}$$

The small disturbance was given by the solution of a linear stability analysis. The Orr-Sommerfeld equation was solved, as described in the next section, and the disturbances were calculated from the resulting eigenfunctions and eigenvalues.

At the wall, no-slip boundary conditions were imposed:

$$u = v = 0. \tag{29}$$

The vorticity at the wall is calculated from the Poisson equation for the normal velocity component, Eq. 4, applied at the wall, where the second derivative of u vanishes:

$$\frac{\partial w_z}{\partial x} = -\frac{\partial^2 v}{\partial y^2}. \tag{30}$$

At the outflow boundary, the following approximations were used:

$$\frac{\partial^2 u}{\partial y^2} = -\alpha_r^2 u', \qquad \frac{\partial^2 v}{\partial y^2} = -\alpha_r^2 v', \qquad \frac{\partial^2 w_z}{\partial y^2} = -\alpha_r^2 w_z'. \tag{31}$$

where the terms u', v' and w_z' are the perturbations at the outflow. This boundary condition represents a periodic disturbances at the outflow with wavenumber α_r, since the second derivative of the mean flow is zero. This boundary condition allows the disturbances to pass through the boundary without reflections. The wavenumber can be computed from the interior solution or, for small wave amplitudes, from a linear stability analysis.

3. Linear stability theory

In order to test the numerical method described above, results for plane Poiseuille flow perturbed by small amplitude periodic disturbances were tested against linear stability results given by a local normal mode analysis based on the Orr-Sommerfeld equations. The problem is illustrated schematically in Fig.(1). The characteristic length scale $\bar{L}$ is half the channel height $\bar{H}$, and the characteristic velocity scale is $\bar{U}(\bar{y} = \bar{H})$.

The linear stability theory assumes that the disturbances propagate n the flow as wave structures with wavenumber α_r, frequency ω, wave speed $c = \omega/\alpha_r$ and growth rate α_i, such that:

$$v'(x, y, t) = v(y) e^{i(\alpha_r x + i\alpha_i) - i\omega t} \tag{32}$$

where, $v'(x, y, t)$ represents the normal component of velocity and $v(y)$ is the complex amplitude distribution. The vorticity disturbance is represented likewise. The Navier-Stokes equations are simplified assuming that the instantaneous velocity can be decomposed into a parallel mean components $U(y)$ and a disturbance. The resulting equation is the Orr-Sommerfeld equation:

$$\alpha(U - c)(v'' - \alpha^2 v) - U''\alpha v = -\frac{i}{Re}(v^{IV} - 2\alpha^2 v'' + \alpha^4 v). \tag{33}$$

The Orr-Sommerfeld equation is an eigenvalue problem which leads to the stability diagram presented in Fig.(2). The neutral curve, for $\alpha_i = 0$ separates the unstable region ($\alpha_i < 0$) from the stable region ($\alpha_i > 0$).

In the present formulation the disturbances grow or decay spatially in the downstream direction. The temporal analysis, where the disturbances grow or decay in time, is much less computationally intensive, but the spatial approach adopted in the present work is more consistent with the flow physics.

Three different test cases where considered. An asymptotically stable case, a neutrally stable case and an unstable case. This cases are indicated in Fig.(2) by points 'A', 'B' and 'C' respectively. The frequencies, wavenumbers and growth rates for these three cases are presented in Table 1.

Table 1: Eigenvalues for the test cases

	A	B	C
Re	5000	10000	10000
α_r	1.157	1.095	1.000
α_i	0.010	0.000	-0.010
ω	0.330	0.270	0.2375

In order to carry out the numerical experiments the laminar Poiseuille flow velocity distribution was perturbed at the inlet boundary. The disturbances initial amplitude was equal to 5×10^{-4}. The spatial evolution of theses disturbances were compared to the corresponding linear stability results at downstream positions. The results are presented in the next section.

4. Numerical results

To carry out the numerical experiments a rectangular domain extending over 8 wavelengths in the streamwise direction was set. The number of grid points taken per wavelength and the number of points in the normal direction were different in each simulation in order to see the results obtained with different spatial discretization methods. The number of grid points per wavelength tested were 7, 8, 16 and 32. In the normal direction 65, 81, 161 and 321 grid points were used. The number of time steps per wave period used was 50 when using 7 or 8 grid points per wavelength and 100 when using 16 or 32 grid points per wavelength.

First the Poiseuille flow was simulated, with a stable, a neutral and an unstable disturbances using a 6^{th} order compact approximation for the spatial derivatives. Fig.(3) shows the comparison of the amplification

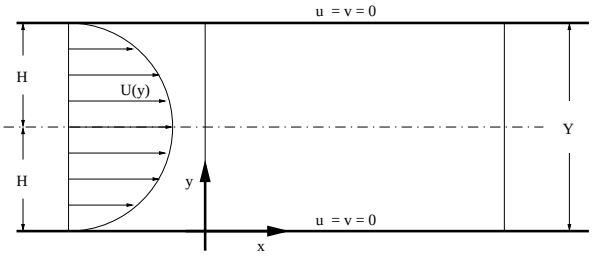

Figure 1: Schematic illustration of the domain and coordinate system for Poiseuille flow stability numerical simulation

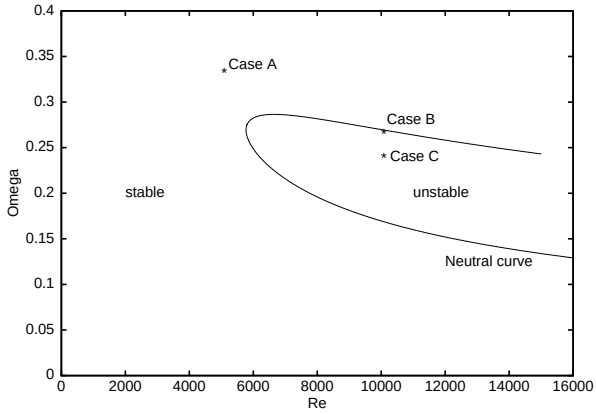

Figure 2: Neutral curve for Poiseuille flow

rates with Linear Stability Theory. The results obtained shows that the 6^{th} order compact approximations is accurate for these cases even with only 7 grid points per wavelength and 65 grid points in the normal direction. The CPU time for this run, in a Silicon Graphics R-10000 workstation, was 1 minute and 39 seconds. Other simulations lowering the number of points in both direction were made, but the results were not accurate. The disturbance velocities and vorticity are plotted in Figs. (4), (5) and (6) for the neutral case.

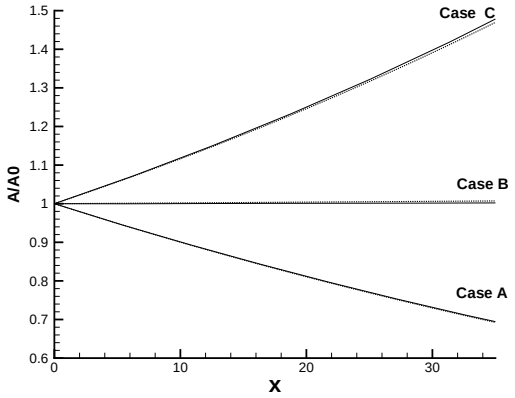

Figure 3: Amplification rates for the three test cases. Comparisons between numerical results (lines) and LST (dots)

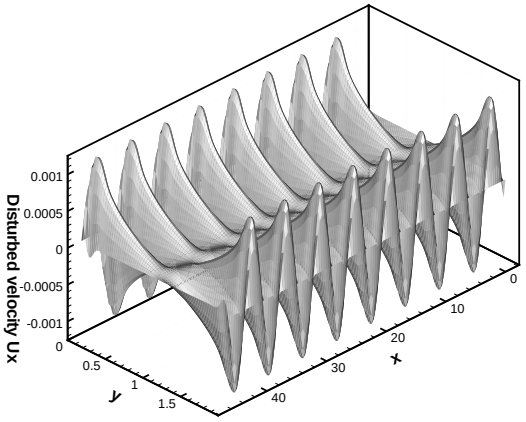

Figure 4: Streamwise disturbance velocity distribution - Numerical results - Test case B

Since the 6^{th} order approximation gives almost the exact answer, the result obtained with this approximations as a reference was taken to access the results obtained with the other discretization schemes. The grid used for the comparisons had 16 points per wavelength and 81 points in the wall normal direction. The test case used to compare the different spatial derivative approximations was the neutral case.

In order to compare the results, the normal component of the disturbed velocity in the middle of the channel was plotted for each test case. There were 8 wavelengths in this computational domain and the amplitude had maximum values equal 5×10^{-4}, since this is a neutral disturbance and this was the amplitude used to disturb the flow.

2^{nd} order approximation. The best result obtained using this approximations were obtained using 32 points per wavelength and 321 points in the normal direction. The total computing time for this simulation was 2 hours 32 minutes and 11 seconds (same workstation Silicon Graphic R-10000). In Fig.(7) one can see that even using this number of points the result obtained was not accurate. This method showed a dissipative behavior. In Fig.(8) 3 other simulations are plotted with different number of points per wavelength and in the normal direction. The plots are shown as N X M where N is the number of points used per wavelength and M is the number of points used in the normal direction. Lowering the number of grid points in the normal direction from 321 to 161, with the same number of grid points per wavelength, results in a stronger dissipation of the wave structure. If the number of grid points per wavelength is reduced to 16 the scheme does not have enough accuracy to resolve the wave structure and a dispersion effect can be observed. The lower the number of grid

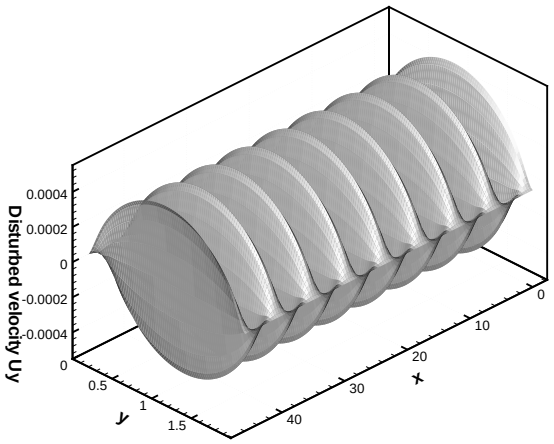

Figure 5: Normal disturbance velocity distribution - Numerical results - Test case B

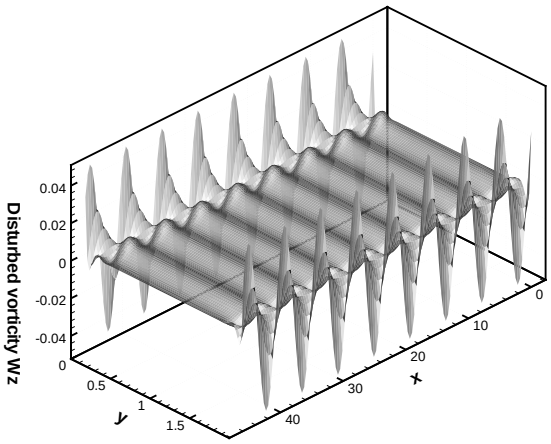

Figure 6: Vorticity disturbance distribution - Numerical results - Test case B

points in the streamwise direction the stronger the phase error.

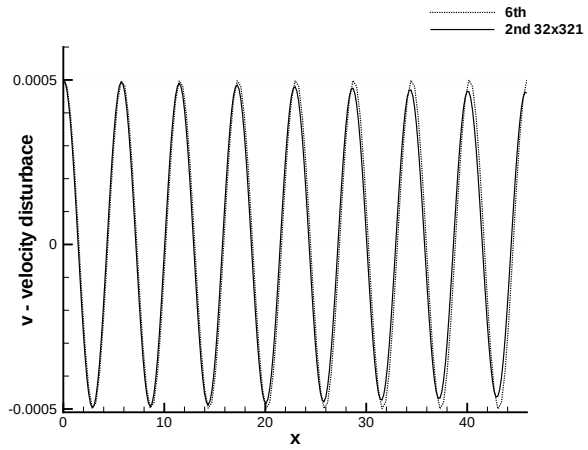

Figure 7: Normal velocity distribution at the middle of the channel along x - comparison 6th X 2nd

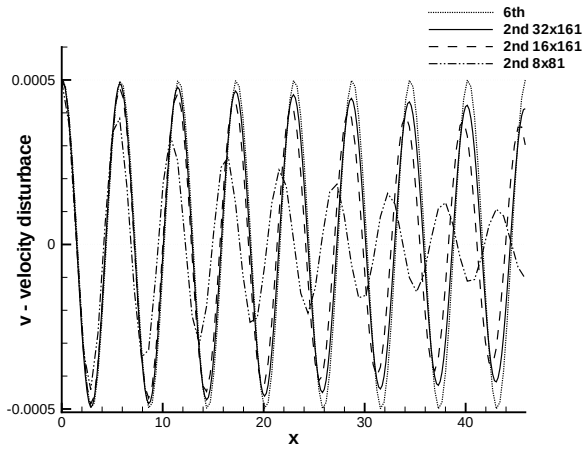

Figure 8: Normal velocity distribution at the middle of the channel along x - comparison 6th X 2nd

4^{th} **order explicit approximation.** The first interesting result that was found was that using a 4^{th} order non-centered approximation for the 2^{nd} derivative for points near the boundary, ($i = 2 and i = N - 1$), an instability was obtained. In Fig.(9) one can observe that the amplitude of the disturbance grow in space when it should remain constant, since a neutral disturbance were simulated. After investigating the possible reasons for this instability, it was found out that replacing the 4^{th} order approximation for the second derivative by a 3^{rd} order approximation this instability was eliminated. Fig.(10) presents the results using a 3^{rd} order approximation for the second derivative near the boundary using 16 points per wavelength and 161 points in the normal direction and the result obtained were in good agreement with the 6^{th} order compact differences results.

In Fig.(11) the results of simulations with different number of points per wavelength and in the normal direction were plotted. Again, one can observe that the number of points per wavelength is related to the phase error of the disturbances and the number of points in the normal direction is related to the accuracy of the grow rate. In order to avoid dispersion error it was necessary to use at least 16 points per wavelength, about twice as much as the number of grid points necessary to have a good resolution with the 6^{th} order scheme.

4^{th} **order implicit (compact) approximations results.** In these simulations one can see that this method was accurate with as little as 8 points per wavelength as shown in Fig.(12). This result was obtained using 161 points in the normal direction. Lowering the number of grid points in the normal direction to 81 introduces dissipation in the solution as shown in Fig.(13). Using the 6^{th} order scheme the number of points in the normal direction can be cut in half to obtain results that are in agreement with LST.

The main advantage of this method, when compared with 4^{th} order explicit method is that one can use less

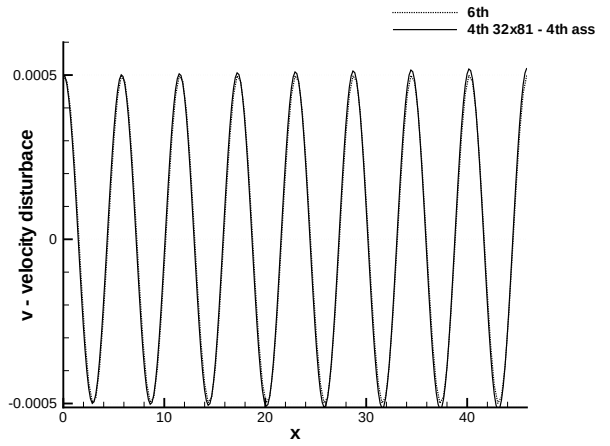

Figure 9: Normal velocity distribution at the middle of the channel along x - comparison 6th order and 4th. 4^{th} order asymmetric at the boundary.

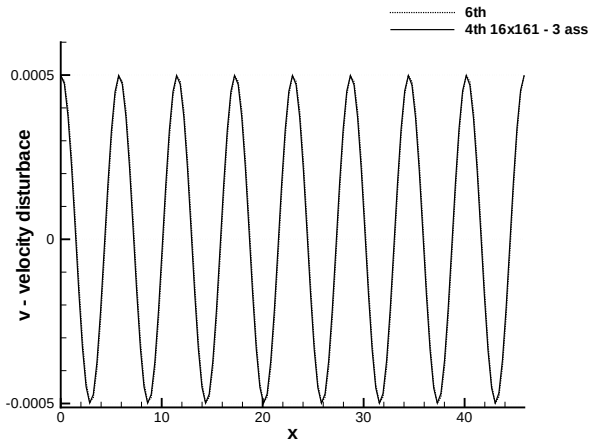

Figure 10: Normal velocity distribution at the middle of the channel along x - comparison 6th order and 4th. 3^{th} order asymmetric at the boundary.

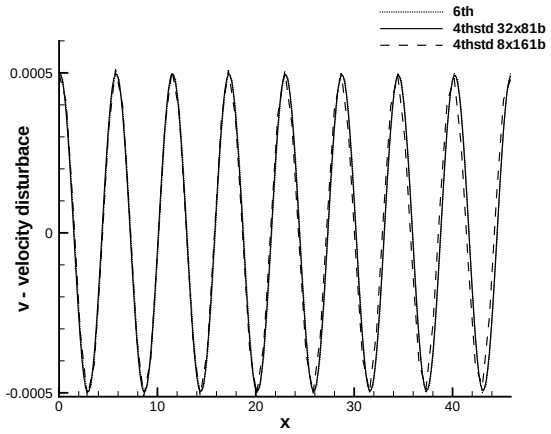

Figure 11: Normal velocity distribution at the middle of the channel along x - comparison 6th order and 4th.

points per wavelength to capture the correct wavelength.

5. Conclusions

In this paper, the influence of the order of spatial derivative approximations on the evolution of stability waves was investigated. The 2^{nd} order approximations was too dissipative and the grid refinement required to obtain reliable results turns this method economically inviable for this kind of study. The result obtained with the finest grid tested with this method took more then 90 times the computational effort of the coarsest grid using 6^{th} order compact approximations, and the result was not good yet.

For the 4^{th} order explicit approximations simulations, one can observe that the number of points required per wavelength was greater then in 4^{th} order compact approximations. Other observation was that non-centered approximations can introduce false flow instability in a simulation, introducing a false amplifications, and this has to be checked when implementing an explicit scheme. In these simulations one can also see that the number of points used per wavelength has a direct connection with the accuracy of the wavelength and the number of points in the normal direction was connected with the accuracy of the growth rate.

The 4^{th} order compact scheme tests shows that the required number of points per wavelength in the case tested (linear grow) can be almost the same as the 6^{th} order compact approximations, but the number of points required in the normal direction was greater, 161 for 4^{th} order compact approximations against 65 for 6^{th} order compact approximations.

The 6^{th} order implicit method employed here shows good agreement with Linear Stability Theory, even using a 'coarse' grid - 7 points per wavelength and 65 points in wall the normal direction.

The main conclusion was that using compact high order schemes for DNS can reduce computational effort

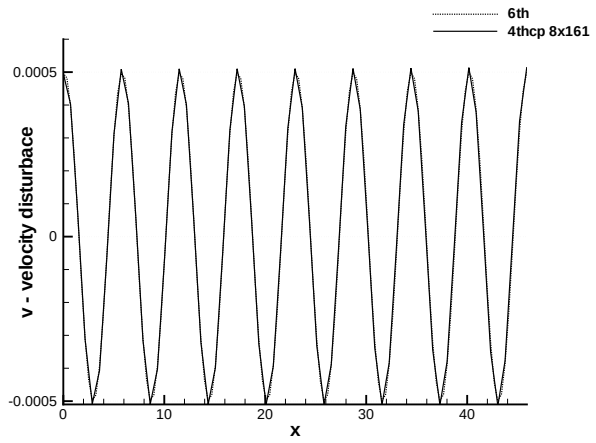

Figure 12: Normal velocity distribution at the middle of the channel along x - comparison 6th X 4th - compact.

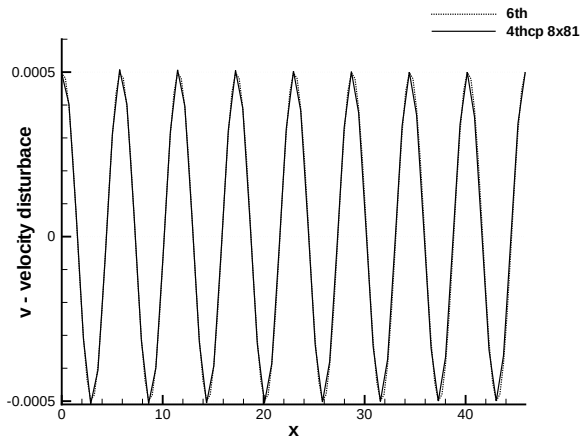

Figure 13: Normal velocity distribution at the middle of the channel along x - comparison 6th X 4th - compact.

and these methods should be used in transitional and turbulent flows simulations were a wide range of length and time scales have to be accurately solved.

6. Acknowledgments

The authors acknowledge the fruitful discussion with Dr. Markus Kloker from University of Stuttgart during the development of the numerical method. The first and the second authors acknowledge the financial support received from FAPESP.

7. references

Adam, Y., 1977, Highly Accurate Compact Methods and Boundary Conditions, "J. Computational Physics", Vol. **24**, pp. 10–22.

Biringen, S. and Laurien, E., 1991, Nonlinear Structures of Transition in Wall-Bounded Flows, "Appl. Num. Mathematics", Vol. **7**, pp. 129–150.

Davies, C., Carpenter, P., and Lockerby, D., 1999, A novel velocity-vorticity method for simulating boundary-layer disturbance evolution and control, "The IUTAM 99 Symp. on Laminar-Turbulent Transition", Arizona, USA.

Ferziger, J. H. and Peric, M., 1997, "Computational Methods for Fluid Dynamics", Springer, Springer–Verlag.

Fezer, A. and Kloker, M., 1999, Spatial Direct Numerical Simulation of Transition Phenomena in Hypersonic Flat-Plate Boundary Layers at Flight Conditions, "The IUTAM 99 Symp. on Laminar-Turbulent Transition", Arisona, USA.

Gmelin, C., Rist, U., and Wagner, S., 1999, DNS of Active Control of Disturbance in a Boundary-layer, "The IUTAM 99 Symp. on Laminar-Turbulent Transition", Arisona, USA.

Guschin, V., Kostomarov, A., Matyushin, P., and Pavlyukova, E., 1999, Direct Numerical Simulation of 2-D/3-D Transition in the Separated Fluid Flows Around a Sphere, "The IUTAM 99 Symp. on Laminar-Turbulent Transition", Arisona, USA.

Hirsh, R. S., 1975, High Order Accurate Difference Solutions of Fluid Mechanics Problems by a Compact Difference Technique, "J. Computational Physics", Vol. **19**, pp. 90–109.

Hu, S. H. and Zhong, X., 1999, Nonparallel Stability Analysis of Hypersonic Flow over a Swept Blunt Leading Edge, "37th AIAA Aerospace Sciences Meeting and Exhibit", Reno, NV.

Joslin, R. D., 1998a, Aircraft Laminar Flow Control, "Ann. Rev. Fluid Mechanics", Vol. **30**, pp. 1–29.

Joslin, R. D., 1998b, Overview of Laminar Flow Control, Technical Report NASA TP-1998-209705, National Aeronautics and Space Administration – NASA.

Laurien, E. and Kleiser, L., 1989, Numerical Simulation of Boundary-Layer Transition and Transition Control, "J. Fluid Mechanics", Vol. **199**, pp. 403–440.

Lele, S., 1992, Compact Finite Difference Schemes with Spectral-like Resolution, "J. Computational Physics", Vol. **103**, pp. 16–42.

Mahesh, K., 1998, A Family of High Order Finite Difference Schemes with Good Spectral Resolution, "J. Computational Physics", Vol. **145**, pp. 332–358.

Messing, R., Kloker, M., and Wagner, S., 1999, Effect of Suction Through Arrays of Holes on a 3-D Boundary Layer Investigated by Spatial Direct Numerical simulation, "The IUTAM 99 Symp. on Laminar-Turbulent Transition", Arisona, USA.

Meyer, D., Rist, U., Gaponenko, V., Kachanov, Y., Lian, Q., and Lee, C., 1999, Late-Stage Transition Boundary-Layer Structures. Direct Numerical Simulation and Experiment, "The IUTAM 99 Symp. on Laminar-Turbulent Transition", Arisona, USA.

Spalart, P. R., 1989, Direct Numerical Study of Crossflow Instability, "The IUTAM 90 Symp. on Laminar-Turbulent Transition", Toulouse, France.

Stemmer, C. and Kloker, M., 1999, Later Stages of Transition of an Airfoil Boundary-Layer Excited by a Harmonic Point Source, "The IUTAM 99 Symp. on Laminar-Turbulent Transition", Arisona, USA.

Wassermann, P. and Kloker, M., 1998, Direct Numerical simulation of the Development and Control of Boundary-Layer Crossflow Vortices, Nilsche, W. and Hilbig, R., editors, "New Results in Numerical and Experimental Fluid Dynamics", Berlin.

Wassermann, P. and Kloker, M., 1999, DNS Investigation of the Development and Control of Crossflow Vortices in a 3-D Boundary-Layer, "The IUTAM 99 Symp. on Laminar-Turbulent Transition", Arisona, USA.

Whang, C. and Zhong, X., 1999, Direct Numerical Simulation of Görtler Instability in Hypersonic Boundary-Layers, "The IUTAM 99 Symp. on Laminar-Turbulent Transition", Arisona, USA.

Zang, T. A., Krist, S. E., and Hussaini, M. Y., 1989, Resolution Requirements for Numerical Simulations of Transition, "J. of Scientific Computing", Vol. **4**, pp. 197–217.

Zhang, H. and Fasel, H., 1999, Spatial Direct Numerical Simulation of Görtler Vortices, "AIAA Fluid Dynamics Conference", Norfolk, USA.

Zhong, X., 1999, DNS of Boundary-Layer Receptivity to Freestream Sound for Hypersonic Flows Over Blunt elliptical Cones, "The IUTAM 99 Symp. on Laminar-Turbulent Transition", Arisona, USA.